Plasma dynamics and self-generated magnetic field distributions in multiple-beam produced plasmas

P M Nilson, L Willingale, M C Kaluza, M S Wei, C Kamberidis, Z Najmudin, W Rozmus, R G Evans [a)], M G Haines, A E Dangor, K Krushelnick

Plasma Physics Group, The Blackett Laboratory, Imperial College, London, SW7 2BZ, UK

R Heathcote, S Bandyopadhyay

Central Laser Facility, CCLRC Rutherford Appleton Laboratory, Chilton, Didcot, Oxon., OX11 0QX, UK

[a)] also at Atomic Weapons Establishment (AWE) plc, Aldermaston, Reading, RG7 4PR

Main contact email address: *philip.nilson@imperial.ac.uk*

Introduction

The importance of self-generated magnetic fields[1)] and heat transport inhibition[2)] in ignition-scale hohlraums[3)] is currently receiving much theoretical attention. Magnetic fields generated at the hohlraum walls may be sufficiently large inside gas-filled hohlraums to affect the electron energy distribution by magnetizing the electrons and reducing the thermal conductivity, altering heater-beam propagation, stability and pointing. In particular, the coupled spatial and temporal evolution of the plasma and the self-generated magnetic fields both inside the hohlraum and at the laser-entrance-holes is not well understood. The role of non-local electron transport, self-generated magnetic fields and heat transport inhibition are therefore important considerations when tuning the hohlraum environment for optimum performance[4)].

Investigations of laser-solid interactions with planar and curved targets in *multiple-beam*, open geometries can somewhat approximate the early-time conditions at the inner wall surfaces of the hohlraum – particularly involving the generation and convection of magnetic fields and the collision of inter-streaming plasma flows.

In this report, we present x-ray imaging measurements of the interaction between two expanding Au plasmas, generated from laser-solid interactions at $1x10^{15}$ Wcm^{-2}. The focal spot separation was varied to alter the collisionality of the interaction. The importance of collisionality on the evolution of the self-generated magnetic fields is discussed.

Experiment

The experiment was performed at the Rutherford Appleton Laboratory using the Vulcan Nd:glass laser (1.054 μm) facility in Target Area West. The targets were Au wires of 1.0 mm diameter, mounted vertically on brass stalks. Two 1.054 μm heater beams, 1 ns in duration, were focused onto target with varying separations (up to 10 times the focal spot diameter) by f/10 lenses, in a focal spot 30-50 μm full width at half-maximum. The average energy per beam was 200 J, giving an on target irradiance of up to $1x10^{15}$ Wcm^{-2}. A diagram of the experimental geometry is given in Figure 1.

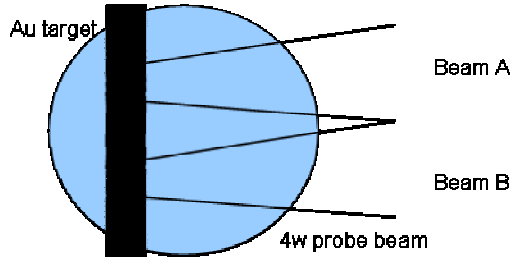

Figure 1. The two beam experimental geometry.

The plasma was diagnosed with a transverse, temporally independent probe beam. The probe beam had 10 ps pulse duration and was frequency quadrupled to 0.263 μm. The refracted probe beam light was re-imaged onto an Andor CCD camera with a magnification of 13x and a micron-scale resolution. A combination of reflective filters and a 4ω interference filter were used to reduce the detectable self-emission from the target.

An x-ray pinhole camera was positioned a few degrees from the target surface normal to monitor the time-integrated emission from the laterally colliding plasmas with 14x magnification. The camera used Kodak DEF film and comprised a 25 μm pinhole and various filters (Be, Mg, Al) sensitive to approximately 1 keV emission.

Results and Discussion

Figure 2 is a typical, time-integrated x-ray pinhole camera image from the experiment. The energies of the two beams for this shot are not equal. The upper beam has approximately half the energy of the lower beam. A distance of 280 μm separated the two focal spots. X-ray emission is evident from both the focal spot regions and the region in between where the plasmas stream into each other. In Figure 4 a), the intensity profile across the two focal spots and the interaction region is plotted. The approximately laminar, central emission region present between the focal spots is likely to be due to the formation of a hydrodynamic shock. In addition, striations of hot plasma are also observable above the filter threshold of 1 keV.

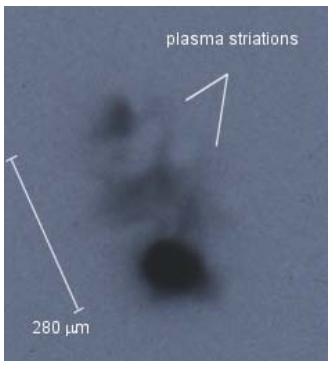

Figure 2. A time-integrated x-ray pinhole camera image. Emission above 1 keV is observed from each of the focal spots and the region of shock formation between the two.

Figure 3 shows the onset of inter-streaming plasma flow for these irradiance conditions from a polarogram taken at t_0 + 400 ps, where t_0 is the initial point of plasma formation. The angle of the analyzer is set to 15 degrees from the crossed-position. Although a discernable magnetic field structure is not evident (likely due to the large angle of the analyser), the plasma dynamics are evident.

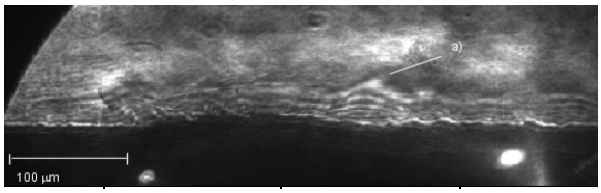

Figure 3. A polarogram of the two beam interaction taken at t_0 + 400 ps. The region of colliding plasmas is marked a).

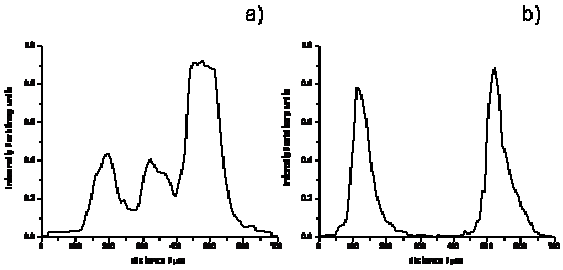

Figure 4. X-ray pinhole camera image profiles for a focal spot separation of 280 μm, a), and 400 μm, b).

The colliding plasma front formed by the closely focused beams in Figure 4 a) is compared, in Figure 4 b), to a shot for a focal spot separation of 400 μm. The energy ratio between the two beams in this case was approximately 1:1. Emission from each of the focal spots is observed, yet there is no detectable emission from between the two. A hydrodynamic shock of sufficient strength to heat the plasma and radiate above 1 keV has not formed.

Various studies have been performed on the inter-penetration and stagnation of supersonic, counterstreaming plasma flows by ablating the surfaces of planar[5] and parallel disks[6]. Various spectroscopic, XUV, x-ray and optical imaging techniques have been used to study their evolution. The introduction of a second laser beam, for our scenario, in planar geometry, introduces a number of interesting complexities. Each focused laser beam generates an ablated plasma plume that expands both normal and parallel to the target surface. In the lateral direction, the interaction will depend upon a number of factors; laser beam timing, laser intensity and wavelength, focal spot size, spot separation, and target composition.

Two limits can be identified on the nature of the interaction. When the ion-ion mean-free path is greater than the characteristic plasma density spatial scale length (low plasma densities), the two plasmas interpenetrate. For small ion-ion mean-free paths in denser regions, however, a shock front will form and the streaming kinetic energy is converted into ion thermal energy. However, the presence of magnetic fields can affect the transport of energy away from the focal spot regions.

The principal mechanism for magnetic field generation arises from the electron pressure gradient term in Ohm's Law.

$$\frac{\partial \vec{B}}{\partial t} = \nabla \times \left(\frac{\nabla p_e}{n_e e} \right) = \frac{k_B \nabla T_e \times \nabla n_e}{n_e e} \qquad (1)$$

Assuming characteristic spatial scale lengths of the order of 10 μm and temperatures of up to 1 keV, megagauss level magnetic fields can be generated on a timescale of 100 ps. Once generated, the magnetic energy increases at the expense of the electron energy, while limited by decreasing temperature and density gradients due to hydrodynamic expansion.

The hydrodynamic expansion of the plasma ablated by a single focused laser beam is dominated by the thermal pressure, i.e. the plasma-β parameter, defined by equation (2), is greater than one.

$$\beta = \frac{P_T}{P_B} = \frac{n_e k_B T_e}{B^2/2\mu_0} \approx 4 \left(\frac{n_e}{10^{20} cm^{-3}} \right) \left(\frac{T_e}{keV} \right) \left(\frac{MGauss}{B} \right)^2 \qquad (2)$$

In the lower density coronal regions, the Hall parameter, defined by equation (3), can be greater than unity, and the magnetic field may play a role in the plasma dynamics by magnetizing the electrons.

$$\omega_c \tau_e = 0.6 \left(\frac{10}{Z} \right) \left(\frac{10^{20} cm^{-3}}{n_e} \right) \left(\frac{10}{\log \Lambda} \right) \left(\frac{T_e}{100 eV} \right)^{3/2} \left(\frac{B}{MGauss} \right) \qquad (3)$$

Consequently, the temperature distribution is modified following the reduction in thermal conductivity, κ.

$$\kappa \approx \left(1 + \omega_c^2 \tau_e^2 \right)^{-1} \qquad (4)$$

For megagauss magnetic fields, $\omega_c \tau_e > 1$ when $T_e > 500$ eV and $n_e > 10^{20}$ cm^{-3}. Hydrodynamics, x-ray emission, parametric instabilities, filamentation and laser beam propagation are all affected by the change in electron energy distribution. Recent hohlraum simulations from the LASNEX code have demonstrated this[7]. A 'localization' effect was observed to affect the electrons, due to the magnetic fields, that reduced the thermal conduction in the axial, cross-field direction.

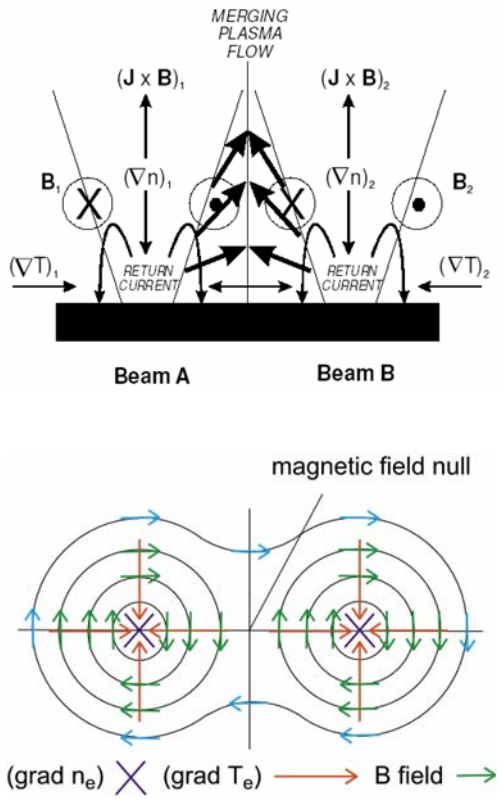

Figure 5. Diagrams of the plasma environment created by two closely focused laser beams.

The collisionality of the interaction as a function of irradiance conditions will affect the generation and evolution of magnetic fields. Each focal spot generates plasma with an associated density and temperature gradient that gives rise to two magnetic fields, B_1 and B_2, as illustrated in Figure 5. The densities, temperatures, and current associated with the central merging plasma will dictate how B_1 and B_2 evolve and decay as they move together.

A similar two-beam geometry to that described above was previously studied by Yates *et al.*[8] with a 10.6 μm wavelength laser. Pinhole camera images showed evidence for remote energy deposition in regions beyond the focal spots. These images were qualitatively understood by the lateral transport of energy by electrons in the magnetic fields generated at the periphery of the laser focal spots. The thermal magnetic waves generated propagate across the target surface until disrupted by, for example, the presence of a second wave from a nearby focal spot. However, there exists between the two focal spots a region of magnetic field null, as depicted in Figure 5. Yates *et al.* noted that the high-energy electron population that transports energy away from the focal spots is magnetically insulated from the target, except at the magnetic field null. Here, the electrons deposit their energy into the target. This was the principal, and only discussed mechanism, for the appearance of significant emission from between the two focal spots.

Importantly, these studies were carried out with high $I\lambda^2$-values, thereby producing a significant population of hot electrons of the order 200 keV. Also, the focal spots were separated by up to 1mm. In our experiments, we will not create a large population of hot electrons due to our reduced $I\lambda^2$. Also, our focal spots are much closer together and more tightly focused by a factor of order two.

We therefore identify three principle mechanisms for x-ray emission from between our focal spots. Firstly, electrons depositing energy into the target in the region of the magnetic field null point. This is likely to be well localized by the geometry of the magnetic fields, yet less important than in the experiments of Yates *et al*. Increasing the focal spot separation will increase the area of the magnetic field null point, reducing the intensity of x-ray emission by this process. This is in agreement with the experimental images, yet does not explain the comparatively large, laminar region of emission observed.

Secondly, we would expect a hydrodynamic shock to be generated where the two laterally expanding plasmas collide. This will result in energy transfer and plasma heating. The closer the focal spots are, the greater the transfer of energy. This may explain the extended, laminar regions of emission in Figure 4 a) and the lack of detectable emission between the focal spots in Figure 4 b), when the focal spots are moved further apart.

Finally, we identify features on the pinhole camera image not directly accountable to the deposition of energy into the target by hot electrons, nor due to the formation of a hydrodynamic shock. In Figure 2, there are striations of plasma emission extending beyond the central region. These do not appear symmetrically around each of the focal spots. We speculate a third process that may give rise to heating and radiative emission. The magnetic fields generated by each of the focal spots will tend to converge upon the magnetic field null over the duration of the pulse. Here, the magnetic field lines of opposite orientation will move towards each other. The closer the focal spots become, the greater the energy density of the magnetic field configuration. In the lower density coronal regions, this is likely to have a greater affect on the electron energy distribution and transport following the increase in the Hall parameter. Energy transfer to the plasma may result in regions of magnetic field annihilation.

Previously, we reported transverse optical probing measurements of the plasma dynamics from Al laser-solid interactions[9], in the above geometry, at $5x10^{13}$ Wcm^{-2}. For these measurements, two heating beams (0.527 μm) were focused to 50-100 μm separation. Using the Faraday rotation technique, possible evidence for magnetic fields were observed after 400 ps. Importantly, by 500 ps, each of the plasmas had expanded into each other, and a qualitatively similar collision to that described above was observed.

Further measurements are required to quantify the magnitude of the magnetic fields in this geometry as a function of irradiance conditions.

Acknowledgements

The authors acknowledge the assistance of the staff of the Central Laser Facility, RAL.

References

1. A Raven, O Willi and P T Rumsby, Physical Review Letters, 41, 8 (1978); M G Haines, 'Magnetic field generation in laser fusion and hot electron transport,' Workshop on the Physics of Laser Fusion, Vancouver BC (1985); A R Bell, Laser Plasma Interactions 5, Proceedings of the 45th Scottish Universities Summer School in Physics, 1994, ed Hooper, IoP Publishing; J A Stamper *et al.*, Physical Review Letters, 26, 1012 (1971); D G Colombant and N K Winsor, Physical Review Letters, 38, 697 (1977); R S Craxton and M G Haines, Physical Review Letters, 35, 20 (1975); M G Haines, Physical Review Letters, 47, 13 (1981); M G Haines, Physical Review Letters, 78, 2 (1997)
2. D S Montgomery *et al.*, Physical Review Letters, 73, 2055 (1994); C A Back *et al.*, Physical Review Letters, 77, 4350 (1996); S H Glenzer *et al.*, Physics of Plasmas, 2117 (1999)
3. J Nuckolls *et al.*, 'Laser compression of matter to super-high densities: thermonuclear applications,' Nature, 239(129) (1972)
4. J Lindl, 'Development of the indirect-drive approach to inertial confinement fusion and the target physics basis for ignition and gain,' Physics of Plasmas 2, 3933 (1995); J Lindl *et al*, 'The physics basis for ignition using indirect-drive targets on the National Ignition Facility,' Physics of Plasmas 11, 339 (2004)
5. J Harilal *et al.*, Journal of Applied Physics, 89, 9 (2001)
6. R A Bosch *et al.*, Phys. Fluids B 4, 4 (1992)
7. R Town, APS Conference Presentation (2004) & private communication
8. M A Yates *et al.*, Physical Review Letters, 49, 23 (1982)
9. P M Nilson *et al.*, RAL Annual Report 2003-2004, p51